Journal of Solid State Chemistry **166,** 118–127 (2002)
doi:10.1006/jssc.2002.9567, available online at http://www.idealibrary.com on IDEAL®

Interplay between Cu and Fe Valences in $BaR(Cu_{0.5}Fe_{0.5})_2O_{5+\delta}$ Double Perovskites with R = Lu, Yb, Y, Eu, Sm, Nd, and Pr

J. Lindén

Department of Physics, Åbo Akademi, FIN-20500 Turku, Finland
E-mail: jlinden@aton.abo.fi

M. Kochi

Materials and Structures Laboratory, Tokyo Institute of Technology, Yokohama 226-8503, Japan

K. Lehmus

Laboratory of Inorganic and Analytical Chemistry, Helsinki University of Technology, FIN-02015 Espoo, Finland

T. Pietari

Department of Technical Physics, Helsinki University of Technology, FIN-02015 Espoo, Finland

and

M. Karppinen and H. Yamauchi

Materials and Structures Laboratory, Tokyo Institute of Technology, Yokohama 226-8503, Japan
E-mail: karppinen@rlem.titech.ac.jp

Received September 5, 2001; in revised form January 28, 2002; accepted March 1, 2002

We have conducted a systematic ^{57}Fe Mössbauer study on $BaR(Cu_{0.5}Fe_{0.5})_2O_{5+\delta}$ double perovskites with various oxygen contents and rare-earth elements (R = Lu, Yb, Y, Eu, Sm, Nd, and Pr). In samples based on R = Lu, Yb, Y, Eu, Sm the oxygen content remained at $\delta \approx 0$, upon reductive or oxidative heat treatments under normal pressure. The larger rare-earth elements, i.e. Nd or Pr, readily allowed for continuous oxygen content tuning up to $\delta \approx 0.3$. By employing high-pressure heat treatments higher oxygen contents were achieved for all samples. The Néel temperature of the samples was found to decrease with increasing amounts of oxygen entering the lattice. In high-pressure oxygenated samples the decrease was less severe indicating that despite the incorporation of oxygen a large amount of Fe still remains in the high-spin trivalent state. By using charge-neutrality arguments together with the relative intensities of the Mössbauer spectral components the average valences of Fe and Cu were obtained. Oxygenation under normal pressure led to a corresponding increase of the valence of Fe, while Cu remained divalent. Upon high-pressure heat treatment equal amounts of Fe^{3+} and Cu^{2+} were found to be oxidized to Fe^{5+} and Cu^{3+}, respectively. © 2002 Elsevier Science (USA)

1. INTRODUCTION

The $LaCuO_{3-y}$ perovskite can be considered as a parent structure for the superconducting cuprate phases. If the A site is co-occupied by a small R (R = rare-earth element; e.g. Y) and a large A metal (e.g. Ba), ordering rather than solid solubility of the R and A atoms is expected, leading to the formation of a double-perovskite structure. This was accomplished for the first time by Er-Rakho *et al.* (1) who found an oxygen-deficient double-perovskite, $BaY(Cu_{0.5}Fe_{0.5})_2O_{5+\delta}$. Later the $BaR(Cu_{0.5}Fe_{0.5})_2O_{5+\delta}$ phase was synthesized also for R = Pr, Nd, Sm, Gd, Dy, Tm and Lu (2). In the structure of $BaY(Cu_{0.5}Fe_{0.5})_2O_{5+\delta}$ barium and yttrium are ordered along the c-axis making the two $(Cu,Fe)O_2$ planes, consisting of the basal planes of $(Cu,Fe)O_5$ pyramids, mirror images for each other. Barium (coordination number CN = 12) in the single BaO plane shares the apical oxygen atoms of the both $(Cu,Fe)O_2$ planes, while yttrium (CN = 8) faces the basal planes of the $(Cu,Fe)O_5$ pyramids. Within the $(Cu,Fe)O_2$ planes copper and iron are not ordered but randomly distributed (3–5).

0022-4596/02 $35.00

The relevant space group is thus $P4/mmm$, in which the Fe and Cu atoms occupy a single lattice site, but with a small systematic splitting between the positions of the two atoms.

The perovskite-derived structures of superconductive cuprates consisting of alternating $M_mO_{m\pm\delta}$ blocks, AO layers and $Q_{n-1}Cu_nO_{2n}$ blocks are classified as members of various $M_mA_2Q_{n-1}Cu_nO_{m+2+2n\pm\delta}$ or $M-m2(n-1)n$ homologous series (6). If the same notation system for the BaR($Cu_{0.5}Fe_{0.5}$)$_2O_{5+\delta}$ double-perovskite structure is applied, it can be expressed as 0112 (7). Note that, the simple perovskite $LaCuO_{3-y}$ would be the $n=1$ member, i.e. 0101, of the same $01(n-1)n$ series. Even though the so-called $02(n-1)n$ (8) series has been found to superconduct, the $01(n-1)n$ series has not been synthesized with superconducting properties yet.

In the BaR(Cu,Fe)$_2O_{5+\delta}$ system, the not-yet-obtained Fe-free phase (9) would be a good candidate for an almost isotropic superconductor, while for the recently stabilized Cu-free phases (10) interesting properties, due to a fluctuating mixed-valence state of iron, were observed (11). In this system, it was shown that five-coordinated Fe^{2+} and Fe^{3+} share an electron, with the result that both formally appear as $Fe^{2.5+}$. Furthermore, for such mixed-valent phases magnetoresistance was recently observed (12).

A systematic study of the oxygen non-stoichiometry in the BaR($Cu_{0.5}Fe_{0.5}$)$_2O_{5+\delta}$ phase has been reported earlier (13, 14). For rare-earth elements smaller than Nd the oxygen content remains constant upon normal pressure O_2/Ar heat treatments. High-pressure heat treatments, on the other hand, were found to increase the amount of excess oxygen, δ. The use of larger rare-earth elements, i.e. Nd or Pr, enables direct variation in oxygen stoichiometry depending on the temperature and the partial pressure of oxygen in the surrounding atmosphere, during the heat treatments. In this paper, evidence is presented for the dependence of Cu valence on the pressure during oxygenation.

2. EXPERIMENTAL

BaR($Cu_{0.5}Fe_{0.5}$)$_2O_{5+\delta}$ samples with R = Lu, Yb, Y, Eu, Sm, Nd, and Pr were prepared from stoichiometric mixtures of $BaCO_3$, R_2O_3 (Pr_6O_{11}), Fe_2O_3 and CuO by heating at 1000°C in air for several days. The normal-pressure oxygenative and deoxygenative post-annealings were carried out for the as-synthesized samples in a thermobalance (Perkin-Elmer System 7 TGA) by heating a sample of $\sim$35 mg at a slow rate of 1°C/min under O_2 and Ar atmospheres. The high-pressure heat treatments were performed on the oxygenated samples in a cubic-anvil-type apparatus at 5 GPa and 1200°C for 30 min. For these experiments powder samples of $\sim$70 mg were separated and tightly packed into gold capsules of 4 mm diameter and 3.7 mm height. Each gold capsule was covered by an NaCl separator and placed into a pyrophyllite container with an internal graphite tube heater. Additionally, one deoxygenated Pr-based sample was heat treated at a high pressure. The high-pressure heat-treated samples are henceforth referred to as HP samples, while the ones oxygenated or deoxygenated under normal pressure are denoted NP samples. In order to improve legibility the "NP" attribute is omitted in the tables for all the normal-pressure samples. Each sample was checked for phase purity and the lattice parameters by X-ray diffractometry using Cu$K\alpha$ radiation. The absolute oxygen content of the samples was determined by both coulometric Cu(I)/(II) titrations and thermogravimetric reduction experiments.

The dc magnetization of the samples was measured under an applied field of 1 T with a SQUID magnetometer (Quantum Design MPMS-5S) in the temperature range of 5–300 K and with a magnetic balance apparatus based on the Faraday method in the temperature range of 300–600 K.

The ^{57}Fe Mössbauer spectra of the samples were recorded at room temperature and at 77 K in transmission geometry. Selected samples were additionally measured at 320–380 K. One of the Pr-based samples was also measured at 10 K in order to get better resolved data and saturated internal field values. Absorbers were made by spreading the sample material mixed with varnish evenly on an Al foil. The thickness of the sample material (expressed in mass per area) was 20 mg/cm^2. A linear Doppler velocity sweeping from -15 to $+15$ mm/s was used when measuring the antiferromagnetic (AF) samples. The paramagnetic (P) samples were scanned with a velocity ranging from -3 to $+3$ mm/s. An Amersham ^{57}Co:Rh (20 mCi, December 1998) source was used for producing the Mössbauer γ quanta, during the time interval of February 1999–January 2001. The spectra exhibiting magnetic splitting were fitted with the full Hamiltonian of combined electric and magnetic interactions. The following hyperfine parameters were included in the fit: the internal magnetic field experienced by the Fe nucleus (B), the chemical isomer shift relative to α-Fe (S), the quadrupole coupling constant (eQV_{zz}), the resonance line widths (Γ), and the relative intensities of the components (I). When fitting paramagnetic spectra B was fixed to zero, the following conditions and constraints were applied: (i) For each component a certain variation in the parameter B was allowed in order to simulate the fact that the internal fields have a certain spread due to, e.g., local distortions of the coordination polyhedra initiated by the random distribution of Fe and Cu atoms at the transition metal site. A Gaussian distribution was assumed and its width (ΔB) was introduced as a fit parameter. (ii) The asymmetry parameter η and the angle θ between the direction of the magnetic and the electric quantization axes were set equal to zero. Attempts to release constraint (ii) did not improve the fittings, as the quadrupole coupling constant in most cases was found to be close to zero, or the intensity of the components so low that lines 3 and 4 of the magnetic sextets were not visible. (iii) All components

were constrained to have equal line widths Γ. (iv) A small asymmetric quadrupole component, originating from traces of iron in the Be detector window and in the Al foil was kept fixed during the fits. These impurity defects cover less than ~2 % of the spectral intensity obtained in the measurements. In the analysis of the P spectra constraint (i) was changed so that B and ΔB were set equal to zero and a small variation of eQV_{zz} was allowed, by introducing a Gaussian with the width ΔV_{zz} as a fit parameter.

3. RESULTS

The samples adopted the tetragonal double-perovskite structure for all rare-earth elements used in the present work. Both lattice parameters, a and c, for the $BaR(Cu_{0.5}Fe_{0.5})_2O_{5+\delta}$ phase increase linearly with the ionic radius of the rare-earth element, whereas introduction of excess oxygen leads to a shrinkage of the unit cell. In Table 1 the lattice parameters are presented. In the samples with R = Lu, Yb, Y, Eu and Sm the amount of excess oxygen δ in the as-synthesized samples was close to zero. As-synthesized samples with R = Nd and Pr on the other hand were found to exhibit oxygen stoichiometries between those of the fully oxygenated and the fully deoxygenated forms. The amount of excess oxygen could thus be tuned in a continuous way from $\delta \approx 0$ to a maximum value, δ_{max}, where $\delta_{max} = 0.25$ and 0.30 for R = Nd and Pr, respectively. High-pressure heat treatments constantly resulted in elevated oxygen contents ranging from $\delta \approx 0.16$ for Y and Yb to $\delta \approx 0.45$ for Pr and Nd. The origin of the excess oxygen is believed to be in hydroxyl groups of the pyrophyllite used as a pressure-transmitting medium and cannot be tuned in a controlled manner, i.e. the final value of δ was found to vary somewhat from one experiment to another.

Before presenting the results obtained by Mössbauer spectroscopy it is useful to review some of the earlier findings. All previous Mössbauer studies on $BaR(Cu_{0.5}Fe_{0.5})_2O_{5+\delta}$ samples revealed an intense component assigned to five-coordinated high-spin Fe^{3+}, in accordance with the expected Fe valence and the presence of $(Cu,Fe)O_5$ pyramids in the structure (1–5, 11, 15). This was rather straightforward using the experimental isomer shift and saturation field values of 0.25–0.35 mm/s and ~50 T, respectively. The component was seen both in AF (i.e. low-δ and/or low-T) and P (i.e. high-δ and/or high-T) spectra. In the P spectra the component exhibits a rather low quadrupole splitting (4). In this work the component will be denoted as Component 1. In general, the AF spectra seldom were completely accounted for using Component 1 only, as an asymmetric broadening of the resonance lines was observed. This was originally handled by introducing a satellite component (1) but later by employing a distribution of the hyperfine parameter values (2, 3, 5). We have adopted the former approach in this paper, in order to simplify the fitting. However, the satellite is still considered to have the same crystallographic and coordinational origin as Component 1.

TABLE 1
Lattice Parameters at 295 K of the $BaR(Cu_{0.5}Fe_{0.5})_2O_{5+\delta}$ Samples

R	δ	a (Å)	c (Å)	V (Å^3)
Pr	0.03	3.928	7.761	119.7
Pr	0.35	3.923	7.759	119.4
Pr(HP)	0.40	3.928	7.754	119.6
Pr(HP)	0.45	3.926	7.757	119.6
Nd	0.01	3.921	7.749	119.1
Nd	0.20	3.915	7.741	118.6
Nd	0.25	3.917	7.745	118.8
Nd(HP)	0.49	3.919	7.733	118.8
Sm	0.03	3.906	7.714	117.7
Eu	0.02	3.899	7.705	117.1
Y	0.03	3.878	7.672	115.4
Y(HP)	0.16	3.873	7.650	114.8
Yb	0.00	3.857	7.641	113.7
Yb(HP)	0.16	3.857	7.626	113.4
Lu	0.01	3.855	7.642	113.6
Lu(HP)	0.36	3.855	7.629	113.4

Note. The statistical error is typically 0.002 Å, 0.15 Å^3, and 0.02 for the lattice parameters, unit cell volume, and δ, respectively. Only high-pressure sample are marked with HP.

The situation becomes more complicated when oxygen is introduced into the lattice. There are not so many reports on oxygen-loaded samples, as only Nd- and Pr-based samples allow for substantial oxygen uptake under ambient pressure (13, 14). Upon oxygenating the samples presence of oxidized Fe species, exhibiting internal fields below that of high-spin Fe^{3+} and negative isomer shift values, are expected. This was indeed observed by Pissas *et al.* (4) who report presence of six-coordinated Fe^{5+} with a saturation fields of 31–34 T and isomer shifts of ~0.0 mm/s in samples with $\delta = 0.26$ and 0.5. Their high oxidation state is in accordance with the oxygen contents and component intensity, as obtained from the computer fittings. Oxidized Fe species are seen in the present samples as well and we have denoted them as Component 3a and 3b in the Mössbauer spectra. In our earlier study traces of oxidized Fe were also found in Mössbauer spectra of $BaY(Cu_{0.5}Fe_{0.5})_2O_{5+\delta}$. These were assigned to six-coordinated Fe^{4+} (9). In addition to this Pissas *et al.* (4) reports for the Pr-based samples a prominent component of an Fe species assigned to valence state +3 based on the isomer shift and internal field values. The component is present also in the paramagnetic phase and they assign it to five-coordinated Fe^{3+}. Thus, one is tempted to equate this component with the satellite of Component 1. However, one additional component, seen mainly in high-pressure treated Y-based samples has been reported (5, 9). It has an isomer shift typical of Fe^{3+} and

reaches its saturation field of more than 50 T already at 300 K and can thus hardly be considered a satellite of Component 1. Its 1st and 6th lines appear in the room-temperature spectra outside the 1st and 6th lines of Component 1 and is assigned to six-coordinated Fe^{3+}, i.e. Fe atoms which are located next to the up-taken extra oxygen, but which for some reason have retained their valence. In this work this component is denoted as Component 2. Although no one else has reported Component 2, it can be observed in e.g. the Mössbauer data of Tm- and Gd-based samples (2), where it has been left unfitted.

As mentioned above only Pr and Nd allow for substantial oxygen loading. However, the choice of rare-earth element affects also the magnetic properties. At 300 K the weakest fields were obtained for the BaR($Cu_{0.5}Fe_{0.5}$)$_2O_5$ phases with the largest R elements and these phases also have the lowest Néel temperatures T_N, as shown by a temperature scan performed by Pissas *et al.* (2).

For the present samples ^{57}Fe Mössbauer spectroscopy data revealed that the oxygenated forms of the phases with R = Nd and Pr are paramagnetic at room temperature, while the deoxygenated samples ($\delta \approx 0$) and HP samples based on Y, Yb and Lu are AF at room temperature. All spectra are dominated by Component 1, in accordance with the previous results. Upon cooling the samples down to 77 K the resonance line width decreases and the internal field of the Component 1 approaches the saturation value of more than 50 T, with a simultaneous weakening of the satellite intensity. The 50 T field and the isomer shift value $S \approx 0.35$ mm/s of Component 1 are typical of high-spin Fe^{3+}, thus confirming the assignment. Generally, the 77 K AF spectra were more reliable for component assignments due to the decreased line widths and increased internal field values. A consistent component assignment can, nevertheless, be achieved for all spectra regardless of the temperature and magnetic state (P/AF ordering). In Figs. 1, 2, and 3 AF Mössbauer spectra recorded at 10, 77, and 300 K, respectively, are shown. The hyperfine parameters obtained from the fittings of the AF spectra are presented in Tables 2 and 3.

In the following, we will review all the other components observed in the low-temperature measurements. When necessary reference to the 300 K spectra is made. The satellite of Component 1 has an isomer shift of $\sim$0.40 mm/s and

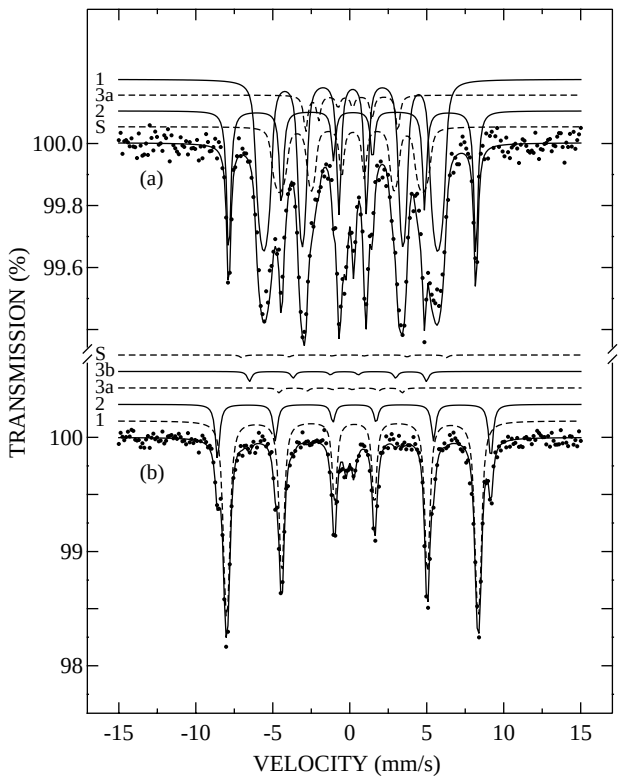

FIG. 1. ^{57}Fe Mössbauer spectra of two AF HP heat-treated BaPr($Cu_{0.5}Fe_{0.5}$)$_2O_{5+\delta}$ samples. Spectrum (a) was recorded for the $\delta = 0.40$ sample at 10 K. Spectrum (b) was recorded for the $\delta = 0.45$ sample at 77 K. The computer fitting is based on Components 1, 2, 3a, 3b and the satellite of Component 1, as explained in the text. The components with appropriate labels are displayed above each spectrum, where S denotes the satellite.

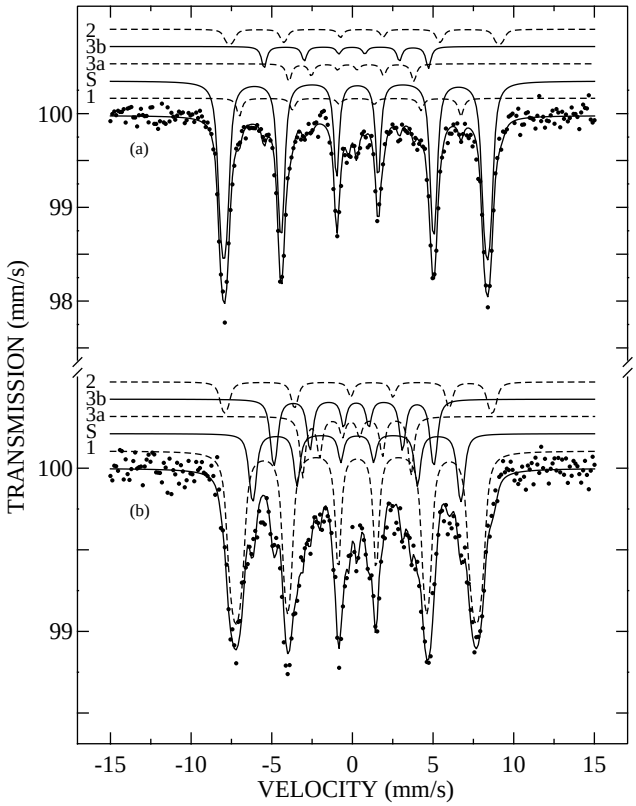

FIG. 2. ^{57}Fe Mössbauer spectra of the AF HP heat-treated BaLu($Cu_{0.5}Fe_{0.5}$)$_2O_{5.36}$ sample, recorded at (a) 300 K, (b) 77 K. The computer fitting is based on Components 1, 2, 3a, 3b and the satellite of Component 1, as explained in the text. The components with appropriate labels are displayed above each spectrum, where S denotes the satellite.

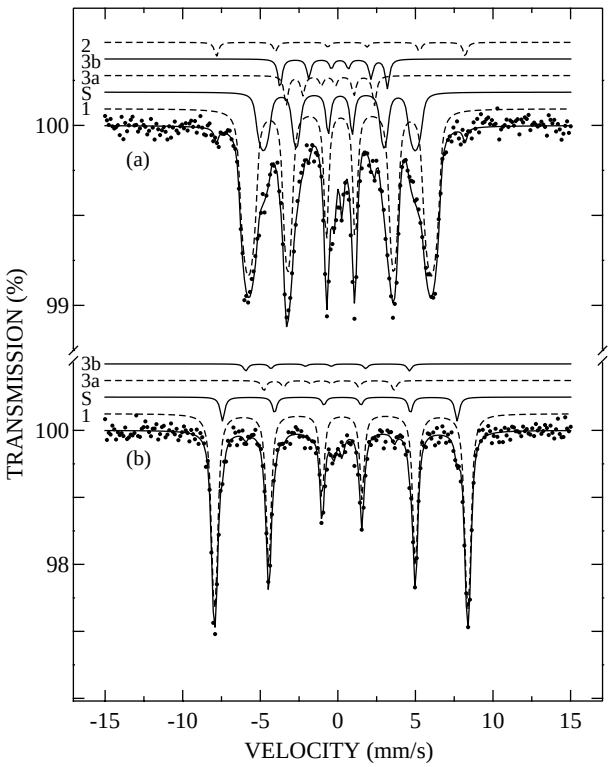

FIG. 3. ^{57}Fe Mössbauer spectra of the AF NP $BaEu(Cu_{0.5}Fe_{0.5})_2O_{5.02}$ sample, recorded at (a) 300 K, (b) 77 K. The computer fitting is based on the Components 1, 2, 3a, 3b and the satellite of Component 1, as explained in the text. The components with appropriate labels are displayed above each spectrum, were S denotes the satellite.

a field of around 45 T. It is thus quite compatible with CN = 5 Fe^{3+} of Component 1. In Figs. 1–3, the satellite is located in the inner slopes of lines 1 and 6 of Component 1. Component 2 has the largest internal field and is usually completely resolved from Component 1, except when R = Pr, and Nd. It exhibits isomer shift values of 0.3–0.5 mm/s, with the exception of two Pr spectra. It is therefore consistent with the CN = 6 Fe^{3+} assignment, as discussed above. (5, 9) It typically gives very sharp peaks to the extreme left and right of the spectra. This is particularly true at 300 K, since upon increasing the temperature the field of Component 1 weakens faster than that of Component 2, cf. Figs. 1a, 1b and 3a. In the 77 K spectrum of Fig. 1b Component 2 is slightly overlapping with Component 1, but still visible enough to enable fitting. This is not the case for spectrum 3b, in which Component 2 could no longer be fitted, although it was quite visible in the 300 K spectrum. In the case of Pr and Nd, Component 2 interferes with Component 1. This is still a problem at 77 K and therefore one of the Pr HP sample was measured at 10 K. In most cases only line 6 of Component 2 is visible in the outer slope of Component 1. This explains the abnormally high isomer shift values of some of the Pr spectra, cf. Table 2.

In addition to the components assigned to Fe^{3+}, one to two less-intense components are discernible in the AF spectra. These components are labeled 3a and 3b. These two components have saturation fields $B \approx 24$ and 34 T, together with substantial negative isomer shifts and are thus readily assigned to oxidized Fe species with the coordination number six. Fe^{3+} species in the intermediate spin state are not considered here, as the excess oxygen present in the phase indicates that oxidized Fe species should be found. In the earlier reports only one such component was detected (4, 5, 9). The rich, but weak structure between the 2nd & 3rd and 4th & 5th lines of Component 1, forced us to introduce Component 3b. The 10 K Pr spectrum could not be fitted in a satisfactory manner using only Component 3a. At 300 K the hyperfine parameter values of Components 3a and 3b do not differ much as these are not so well resolved from each other due to line broadening, Table 3. The total amount of oxidized Fe in the Mössbauer spectra remains roughly the same, whether one is fitting the spectra using one or two components. This is due to the fact that Components 3a and 3b do not overlap strongly with Components 1 and 2, owing to their differences in internal field values. Components 3a and 3b interfere with each other, which results in the scattering of the isomer shift and quadrupole coupling constant values. However, in the following section we will be mainly interested in the overall intensity of Components 3a and 3b. In our earlier works the observed Component 3a was assigned to high-spin Fe^{4+}, but with the present results of the highly oxygenated samples at hand the pentavalent state seems more probable, in accordance with Ref. (4). The valence state will also be discussed further on. At this point it is enough to notice that particularly in the oxygenated samples, surprisingly small amounts of oxidized Fe is found. Assuming the tetravalent state for Components 3a and 3b, would force us to increase the valence of the Cu atoms to almost + 3, which seems highly improbable. Only for the samples with a low oxygen content could Fe^{4+} species be considered.

The paramagnetic spectra were analyzed using three spectral components. Typical spectra obtained for NP and HP paramagnetic samples are shown in Figs. 4 and 5. Hyperfine parameters obtained from the fittings are given in Table 4.

Some of the spectra (including that for the Lu(HP) $\delta = 0.36$ sample) were recorded at elevated temperatures in order to get pure paramagnetic hyperfine parameter values above T_N. The component with the smallest value for the isomer shift (Component 3, $S \approx 0.0$ mm/s) is readily assigned to six-coordinated Fe in an oxidized state in accordance with results from the AF spectra and Ref. (4). As suggested above the valence is tentatively assigned to + 5. The two other components have isomer shift values S = 0.25–0.30 mm/s, i. e. typical of Fe^{3+} with coordination numbers five and six. These two components differ in the

TABLE 2
Hyperfine Parameters Obtained from the Fittings of the 77 K Antiferromagnetic Mössbauer Spectra

		Intensities (%)				Internal fields (T)			
R	δ	I_1^a	I_2	I_{3a}	I_{3b}	B_1	B_2	B_{3a}	B_{3b}
Pr	0.03	87(3)	6(1)	4.1(7)	2.9(7)	49.35(4)	53.3(3)	23.6(5)	32.5(5)
Pr(HP)	0.40	81(4)	4(3)	8.6(8)	6.7(9)	48.1(3)	51(1)	23.1(2)	33.5(3)
Pr(HP)[b]	0.40	85(2)	4.3(9)	4.8(7)	5.6(7)	50.62(4)	53.0(2)	24.2(3)	31.7(3)
Pr(HP)	0.45	71(2)	7(1)	9.2(7)	12.8(7)	46.17(9)	51.3(3)	20.8(2)	30.7(2)
Nd	0.01	93(4)	—	4(1)	2(1)	49.86(4)	—	24.2(3)	33.5(8)
Nd	0.25	66(3)	15(2)	11.6(7)	8.3(8)	45.3(2)	47.9(2)	17.9(2)	31.0(4)
Sm	0.03	94(4)	—	3(1)	3(1)	50.29(3)	—	23.9(4)	32.8(4)
Eu	0.02	96(4)	—	2.4(9)	2(1)	50.56(3)	—	24.9(4)	31.9(5)
Y(HP)	0.16	91(3)	3.4(9)	2(1)	3(1)	50.15(3)	54.6(3)	24.4(5)	33.9(4)
Yb	0.00	96(4)	—	1(1)	2(1)	50.96(3)	—	26.9(4)	33.5(5)
Yb(HP)	0.16	86(4)	8(1)	3(1)	5(1)	50.67(3)	53.1(2)	24.5(4)	36.7(3)
Lu	0.01	88(4)	3(1)	4(1)	6(2)	50.8(4)	53.8(6)	25.0(5)	36.5(3)
Lu(HP)	0.36	80(3)	16.3(9)	1.7(7)	2.5(7)	50.66(2)	54.98(6)	25.6(4)	36.1(3)

		Isomer shifts (mm/s)				Quadrupole coupling constants (mm/s)			
R	δ	S_1	S_2	S_{3a}	S_{3b}	eQV_{zz}^1	eQV_{zz}^2	eQV_{zz}^{3a}	eQV_{zz}^{3b}
Pr	0.03	0.365(4)	0.48(3)	− 0.04(6)	− 0.11(7)	− 0.17(2)	− 0.1(1)	− 0.2(3)	− 0.9(3)
Pr(HP)	0.40	0.35(2)	0.3(3)	− 0.14(4)	− 0.07(4)	− 0.2(1)	− 1.3(9)	− 0.2(1)	− 0.1(2)
Pr(HP)[b]	0.40	0.367(4)	0.74(6)	− 0.08(5)	− 0.08(5)	− 0.21(2)	− 0.1(2)	− 0.5(2)	− 0.6(1)
Pr(HP)	0.45	0.371(8)	0.89(5)	− 0.20(5)	− 0.27(2)	− 0.13(3)	− 1.7(2)	− 0.7(2)	− 0.29(8)
Nd	0.01	0.363(5)	—	− 0.01(5)	− 0.1(1)	− 0.10(2)	—	− 0.3(2)	− 1.0(4)
Nd	0.25	0.35(1)	0.38(2)	− 0.11(3)	− 0.06(5)	− 0.16(5)	− 0.07(8)	− 0.9(1)	− 0.7(2)
Sm	0.03	0.366(3)	—	− 0.13(5)	− 0.00(5)	− 0.1(2)	—	− 0.6(2)	− 1.3(2)
Eu	0.02	0.351(3)	—	− 0.18(8)	− 0.29(7)	− 0.09(1)	—	− 0.6(3)	− 1.6(3)
Y(HP)	0.16	0.357(3)	0.56(5)	− 0.0(1)	− 0.33(5)	− 0.26(1)	− 1.7(2)	− 0.6(3)	− 0.5(2)
Yb	0.00	0.341(4)	—	− 0.40(7)	− 0.04(8)	− 0.18(2)	—	− 0.6(4)	− 0.3(3)
Yb(HP)	0.16	0.349(4)	0.52(3)	− 0.49(5)	− 0.53(4)	− 0.22(2)	− 0.7(1)	− 0.1(2)	− 0.7(2)
Lu	0.01	0.351(5)	0.53(7)	− 0.58(6)	− 0.58(5)	− 0.17(2)	− 2.6(3)	− 2.77(2)	− 1.67(2)
Lu(HP)	0.36	0.348(3)	0.406(8)	− 0.39(5)	− 0.39(4)	− 0.26(1)	− 0.04(3)	− 0.1(2)	− 0.7(2)

Note. From the normal-pressure samples the 'NP' notation is omitted.
[a]Includes satellite intensity (when present).
[b]Data obtained at 10 K.

value of the quadrupole coupling constant eQ_eV_{zz}. Upon increasing δ the intensity of the component with a smaller eQ_eV_{zz} value decreases, while the other component increases its intensity. Moreover, as the octahedral coordination polyhedron is somewhat flattened resulting in an increased value for the quadrupole coupling constant, the component with the larger eQ_eV_{zz} value (Component 2) is assigned to six-coordinated Fe^{3+} and the component with the smaller eQ_eV_{zz} value (Component 1) to five-coordinated Fe^{3+}. Earlier high-temperature Mössbauer measurements confirm the assignment of the latter component (4, 15). The results of the paramagnetic spectra agree rather well with the corresponding AF spectra, i.e. there are three types of Fe species: CN = 5 Fe^{3+} (Component 1), CN = 6 Fe^{3+} (Component 2), and CN = 6 Fe^{5+} (Component 3). For Nd and Pr the intensity of Component 2 is lower in the AF phase, which is due to the overlapping of Components 1 and 2, as explained above. The amounts of Fe^{5+} in the P and AF spectra are roughly equal on the other hand. For the Lu(HP) sample Component 2 is well resolved in all the spectra and has therefore approximately constant intensity. Components 3a and 3b appeared rather weak in the corresponding AF spectra, a fact which leads to an under-estimation of the amount of Fe^{5+} for Lu(HP) $\delta = 0.36$ in the AF phase.

With the assignment completed, the intensities of the spectral components in the AF and P Mössbauer spectra can be used for checking the distribution of excess oxygen in the lattice. In particular, we will discuss the fact that the amount of oxidized Fe in HP samples remains below the values predicted by the oxygen contents of the samples, even when presence of oxidized Fe^{5+} is assumed. In order to do

TABLE 3
Hyperfine Parameters Obtained from the Fittings of the 300 K Antiferromagnetic Mössbauer Spectra

		Intensities (%)				Internal fields (T)			
R	δ	I_1^a	I_2	I_{3a}	I_{3b}	B_1	B_2	B_{3a}	B_{3b}
Nd	0.01	94(2)	—	5.6(3)	—	33.45(4)	—	12.2(2)	—
Eu	0.02	88(4)	2.21(5)	4.7(5)	4.6(6)	36.5(1)	49.6(3)	17.6(2)	21.4(2)
Y(HP)	0.16	91(4)	—	9.6(8)	—	31.4(1)	—	17.9(2)	—
Yb	0.00	94(4)	—	6(1)	—	39.9(1)	—	16.4(4)	—
Yb(HP)	0.16	86(3)	7.1(5)	4.1(5)	3.0(6)	36.80(3)	49.6(1)	19.7(3)	27.1(2)
Lu	0.01	87(4)	3.6(5)	5.5(5)	3.5(5)	39.93(7)	49.1(2)	20.8(3)	26.2(2)
Lu(HP)	0.36	76(3)	19.1(6)	5.0(6)	—	35.00(7)	49.73(4)	18.6(2)	—
		Isomer shifts (mm/s)				Quadrupole coupling constants (mm/s)			
R	δ	S_1	S_2	S_{3a}	S_{3b}	eQV_{zz}^1	eQV_{zz}^2	eQV_{zz}^{3a}	eQV_{zz}^{3b}
Nd	0.01	0.351(4)	—	− 0.29(3)	—	− 0.4(1)	—	− 0.94(8)	—
Eu	0.02	0.264(4)	0.51(4)	− 0.44(3)	− 0.04(2)	− 0.11(2)	− 0.9(2)	− 0.25(9)	− 0.80(9)
Y(HP)	0.16	0.276(8)	—	− 0.33(3)	—	− 0.27(3)	—	− 1.59(9)	—
Yb	0.00	0.249(5)	—	− 0.06(4)	—	− 0.08(2)	—	− 0.5(2)	—
Yb(HP)	0.16	0.249(3)	0.32(2)	− 0.29(3)	− 0.50(3)	− 0.23(1)	− 0.12(6)	− 1.9(1)	− 1.8(1)
Lu	0.01	0.247(3)	0.11(2)	− 0.55(4)	− 0.06(3)	− 0.15(1)	− 0.6(1)	− 1.3(1)	− 0.7(1)
Lu(HP)	0.36	0.236(6)	0.296(6)	− 0.02(3)	—	− 0.25(2)	− 0.09(3)	− 0.8(1)	—

Note. From the normal-pressure samples the "NP" notation is omitted.
[a]Includes satellite intensity (when present).

this we will infer a partial oxidation of Cu^{2+} to Cu^{3+}. The discrepancy between the value of δ and the total intensity of six-coordinated Fe in HP samples is clearly visible e. g. for the two spectra of Fig. 5. The relative component intensity corresponding to six-coordinated Fe is smaller for spectrum (b) than for spectrum (a), although the δ value is larger in the (b) case. Possible small variations in the recoil-free fraction for the various Fe species is neglected. This approach is justifiable as we are mainly trying to illustrate the difference between the NP and HP samples, both types of which exhibit a sufficiently broad variation in the oxygen contents. Two models were tested. In Model A, the amount of six-coordinated Fe (i.e. integrated intensity of Components 2, 3a and 3b) is equal to δ. In practice, this means that oxygen fills with equal probability the site between two Cu atoms, two Fe atoms, or a Cu atom and an Fe atom. Inherently, it is assumed that the Cu and Fe atoms populate the transition metal site at random. This has actually been confirmed using convergent-beam-electron diffraction (16). Then according to the binomial distribution 50% of the excess oxygen atoms goes between a Cu atom and a Fe atom, 25% goes between two Fe atoms and another 25% between two Cu atoms. Excess oxygen atoms located between two Cu atoms are not detectable in the Mössbauer spectra. On the other hand, those oxygen atoms, which are located between two Fe atoms, are detected twice. Hence, on the average the amount of six-coordinated Fe reflects the actual value of δ.

In Model B every excess oxygen atom is always sandwiched between a Cu atom and an Fe atom or between two Fe atoms but *not* between two Cu atoms, i.e. only Fe ions may attract excess oxygen atoms. According to this assumption and the binomial model $\frac{1}{3}$ of the excess oxygen atoms are detected twice, predicting a ratio of $\frac{4}{3}$ between the number of six-coordinated Fe atoms and the value of δ.

In a slightly modified Model B (Model B*) the site between two Fe atoms is twice as likely to catch an oxygen atom as compared to the space between a Cu atom and an Fe atom. In this case the ratio between the number of six-coordinated Fe atoms and the number of excess oxygen atoms becomes $\frac{3}{2}$.

In Fig. 6 the amount of six-coordinated Fe vs δ is presented, as obtained from the fit results of the Mössbauer spectra, Tables 2–4. The predictions of Models A and B* are drawn as solid lines. Model A adequately describes the situation for the HP samples while Model B* fits well to the NP sample data.

The results of Fig. 6 also help us to understand the Fe valence as a function of δ. Using the experimentally obtained portions of Fe^{5+} and Fe^{3+} from Tables 2–4 an overall Fe valence in the $BaR(Cu_{0.5}Fe_{0.5})_2O_{5+\delta}$ phase is readily calculated. The result is presented in Fig. 7. Again the NP and HP data follow different trends. Assuming the ordinary integer valence states of R^{3+}, Ba^{2+}, Cu^{2+} and O^{2-}, then that of Fe should be given by $+(3+2\delta)$. This

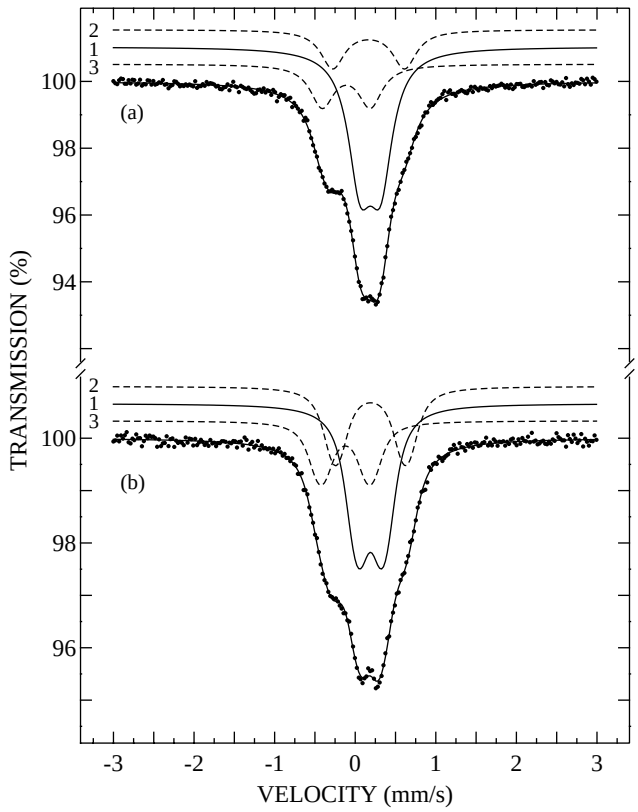

FIG. 4. ^{57}Fe Mössbauer spectra of the paramagnetic BaNd($Cu_{0.5}Fe_{0.5}$)$_2$ $O_{5+\delta}$ samples. Spectrum (a) was recorded for the $\delta = 0.25$ NP sample, at 300 K. Spectrum (b) was recorded for the $\delta = 0.49$ HP sample at 300 K. The components reading from top are: $CN = 6$ Fe^{3+} (Component 2), CN = 5 Fe^{3+} (Component 1), and CN = 6 Fe^{5+} (Component 3).

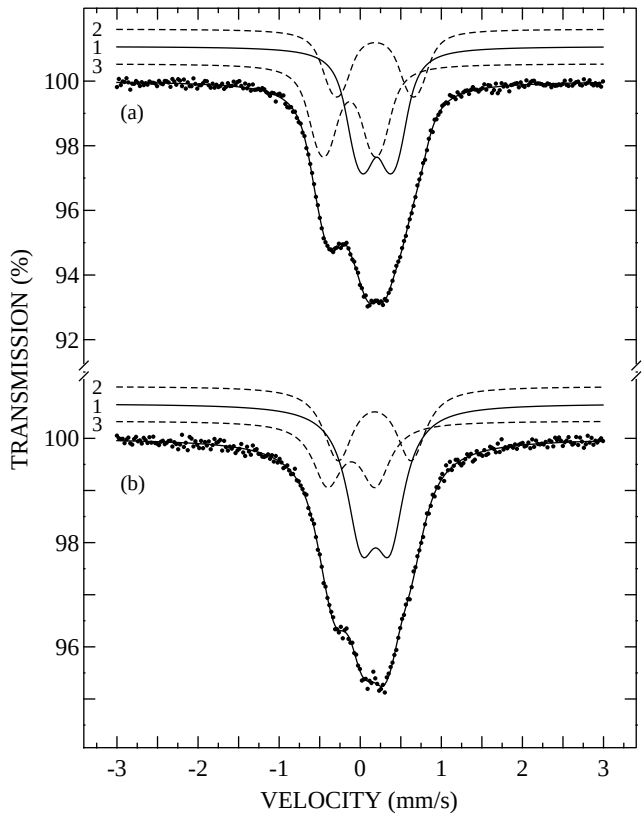

FIG. 5. ^{57}Fe Mössbauer spectra of the paramagnetic BaPr($Cu_{0.5}Fe_{0.5}$)$_2$ $O_{5.25}$ samples. Spectrum (a) was recorded for the $\delta = 0.35$ NP sample at 300 K. Spectrum (b) was recorded for the $\delta = 0.45$ HP sample at 300 K. The components reading from top are: $CN = 6$ Fe^{3+} (Component 2), CN = 5 Fe^{3+} (Component 1), and CN = 6 Fe^{5+} (Component 3).

expression is used for plotting the upper curve of Fig. 7 and it describes reasonably well the trend for the NP samples. For the HP samples the valence states of both Cu and Fe are assumed to depend on δ. The natural choice, based on the distribution of excess oxygen is $+(2+\delta)$ and $+(3+\delta)$, for the valence states of Cu and Fe, respectively. The lower curve of Fig. 7 illustrates the situation for the Fe atoms. Again a reasonable agreement is obtained, although a detailed description would perhaps require a more refined model.

As the Mössbauer spectra revealed presence of AF ordering for all deoxygenated NP samples at 300 K, the transition from the paramagnetic to the AF state could not be observed in the 5–300 K SQUID data. Some samples were thus measured in the 300–600 K interval using a magnetic-balance apparatus in order to find the Néel temperature T_N. It turned, however, out that some of the oxygenated Pr samples did not exhibit a clear transition in the expected region. This is in accordance with earlier reports (4). There may be several reasons for this. First of all the transition region from AF to P is wide. At 300 K e.g. the $\delta = 0.40$ sample is AF, but with extremely broadened lines. The temperature had to be increased up to 355 K before the magnetic features disappeared. Furthermore, the Pr^{3+} ion has a large magnetic moment, which gives a strong paramagnetic background to the susceptibility curves and hampers the detection of the ordering of the Fe spins. Neutron data on the Pr phase also indicates that the magnetic ordering of the oxygenated phase is of rather short range (4). In Table 5, the dependence of T_N for the Pr-based samples, as estimated from the Mössbauer data, in terms of δ is presented. For the NP samples the T_N vs δ relation is decreasing practically linearly. Again the HP samples behave differently, by exhibiting substantially higher T_N values, Table 5.

This difference in the T_N value between HP and NP samples is in accordance with the general findings of the Mössbauer analysis. As high-pressure heat treatment favored the formation of high-spin six-coordinated Fe^{3+} on the expense of high-spin Fe^{5+}, the AF coupling is only slightly affected when oxygen enters the lattice. Normal-pressure oxygenation, on the other hand, leads to the formation of substantial amounts of six-coordinated Fe^{5+} with a spin of $\frac{3}{2}$. This is less than that of high-spin Fe^{3+} (spin = $\frac{5}{2}$). A diminished spin presumably weakens the AF coupling,

TABLE 4
Hyperfine Parameters Obtained from the Fittings of the 300 K Paramagnetic Mössbauer Spectra

R	δ	I_1(%)	I_2(%)	I_3(%)	S_1	S_2	S_3	eQV_{zz}^1	eQV_{zz}^2	eQV_{zz}^3
Pr	0.35	42(2)	25(2)	33(2)	0.319(4)	0.30(1)	− 0.015(5)	0.79(2)	1.90(3)	1.31(1)
Pr(HP)[a]	0.40	53(3)	29(2)	18(3)	0.25(1)	0.24(2)	− 0.03(3)	0.58(3)	1.88(7)	1.0(1)
Pr(HP)[b]	0.45	48(2)	28(1)	24(2)	0.296(6)	0.30(1)	− 0.013(6)	0.69(1)	1.75(3)	1.19(1)
Nd	0.20	60.7(9)	21(1)	19(1)	0.301(3)	0.278(8)	− 0.005(6)	0.502(8)	1.87(3)	1.19(3)
Nd	0.25	60(2)	19(1)	21(1)	0.302(2)	0.280(8)	− 0.003(4)	0.510(7)	1.79(3)	1.19(2)
Nd(HP)	0.49	50(2)	28(1)	22(2)	0.304(3)	0.306(6)	− 0.008(5)	0.636(8)	1.74(2)	1.22(1)
Lu(HP)[c]	0.36	77(2)	11(1)	12(1)	0.235(4)	0.41(1)	− 0.16(2)	0.50(1)	0.92(6)	0.29(7)

Note. The unit of S and eQV_{zz} is mm/s. Unless indicated otherwise $T = 300\ \mathrm{K} > T_N$. From the normal-pressure samples the "NP" notation is omitted
[a]Measured at 355 K
[b]Measured at 310 K
[c]Measured at 380 K.

which explains the lower T_N values of the NP samples as compared to the HP samples.

4. DISCUSSION

Generally speaking, the presence of a certain amount of Cu^{3+} in the HP samples is a direct consequence of the fact that most of the HP Mössbauer spectra exhibit substantial amounts of six-coordinated Fe^{3+}. In other words, upon increasing the coordination number of Fe without increasing its valence, another cation must increase its valence to ensure charge neutrality. In the AF Mössbauer spectra the up to $\simeq 55$ T field and the, in some cases, excellent distinction from the other components makes the assignment of the conspicuous Component 2 (CN 6 Fe^{3+}) unambiguous, see e.g. the spectra of Fig. 1. It is therefore hardly surprising that Component 2 is absent from most of the NP spectra. In previous works dealing with NP samples Component 2 was not reported (2–4, 15) In line with this, in our previous

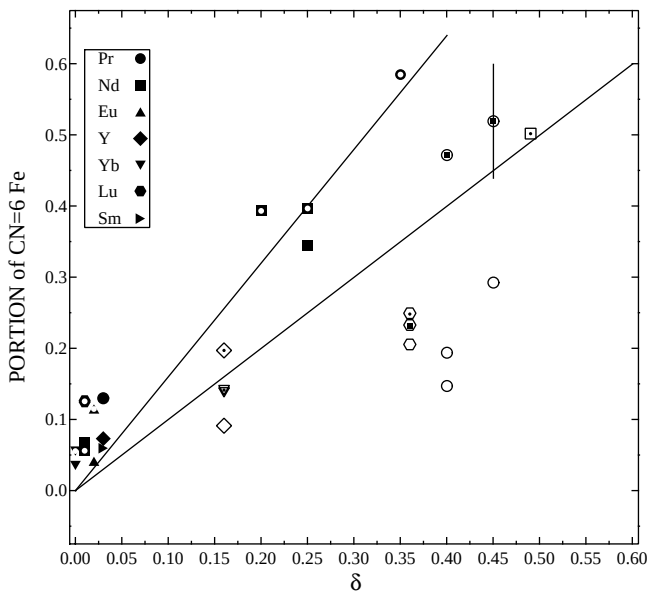

FIG. 6. Portion of six-coordinated Fe vs δ, as obtained from the analysis of the Mössbauer spectra. Filled and open symbols denote normal (NP) and high-pressure (HP) samples, respectively. Dot-centered data points indicate 300 K data. The three square-centered data points were obtained from paramagnetic spectra measured at elevated temperatures, see Table 4. The maximal statistical error is given as an error bar on one of the data points. The theoretical lines illustrate that the portion of six-coordinated Fe depends on the excess oxygen content as $f(\delta) = 3\delta/2$ or $f(\delta) = \delta$, for NP and HP samples, respectively.

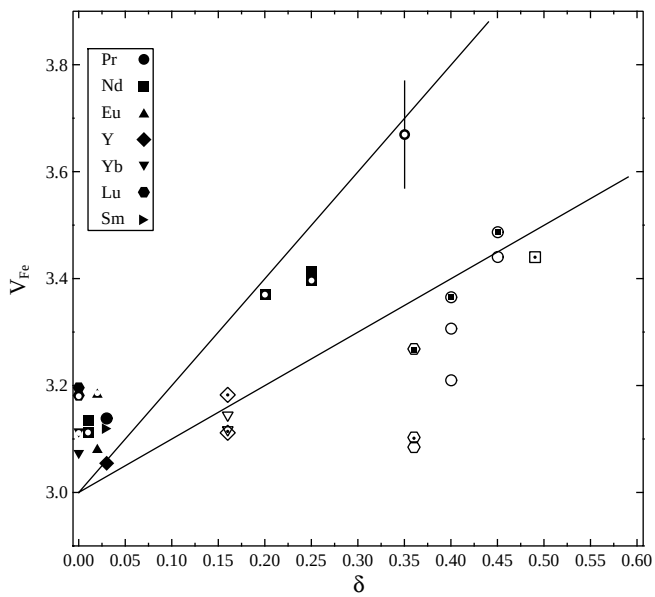

FIG. 7. Average valence of Fe vs δ, as obtained from the analysis of the Mössbauer spectra. Filled and open symbols denote NP and HP samples, respectively. Dot-centered data points indicate 300 K data. The three square-centered data points were obtained from paramagnetic spectra measured at elevated temperatures, see Table 4. The maximal statistical error is given as an error bar on one of the data points.

TABLE 5
Néel Temperature of the $BaPr(Cu_{0.5}Fe_{0.5})_2O_{5+\delta}$ Samples

Synthesis cond.	δ	T_N(K)
NP	0.03	350 ± 20
NP	0.20	295 ± 50
NP	0.35	280 ± 5^a
HP	0.40	360 ± 10
HP	0.45	310 ± 50

[a]Obtained by SQUID measurement

studies a maximum Component 2 intensity of ≈ 22 % was obtained for a HP sample (5, 9). On the other hand, Components 3a and/or 3b are observed in all AF spectra with $\delta > 0$, as shown by Tables 2 and 3. The total intensity of Components 3a and 3b is therefore an interesting parameter, as it reflects the amount of oxidized Fe. The actual hyperfine parameters are less important and the rather scattered isomer shift values should not be used for drawing too far-reaching conclusions. It is enough that the internal field values of Components 3a and 3b clearly separates them from Components 1 and 2.

The origin of the two oxidized Fe species in the Mössbauer spectra is somewhat uncertain. Possibly one of them could represent Fe^{4+} instead of Fe^{5+}. This would give a better agreement between the results of the low-δ Mössbauer spectra and the oxygen content analysis. However, for the HP samples even higher amounts of Cu would have to reside in the Cu^{3+} state.

The change of the crystal c-axis length as a function of δ in ordered perovskite structures depends on the choice of transition metal. Thus in the Cu-based triple-perovskite ($YBa_2Cu_3O_6$) a shrinkage is observed upon oxygen loading (17), whereas the opposite is true for the Fe-based version ($YBa_2Fe_3O_8$) (18). The fact that the c-axis in the present system decreases (Table (1)) as a function of δ is therefore dictated by the Cu atoms. In contrast, oxygen loading of the Cu-free 0112 phase causes an expansion of the c-axis (11).

5. CONCLUSIONS

The $BaR(Cu_{0.5}Fe_{0.5})_2O_{5+\delta}$ double-perovskite structure is stabilized for all R ionic radius ranging from 0.977 to 1.126 Å . Using normal-pressure synthesis the amount of excess oxygen δ, remained close to zero in samples with $R =$ Lu, Yb, Y, Eu and Sm while for $R =$ Nd and Pr substantial amounts of excess oxygen entered the structure upon normal-pressure oxygenation. When oxygen entered the structure at normal pressure the valence of Fe^{3+} (electron spin $\frac{5}{2}$) was found to be raised to Fe^{5+} (electron spin $\frac{3}{2}$), thus weakening the AF coupling. After high-pressure heat treatments a portion of the Cu^{2+} species was oxidized to Cu^{3+}, while a portion of the five-coordinated Fe^{3+} simply became six-coordinated Fe^{3+}. Therefore the AF coupling of the HP samples was less affected. This accounts for the higher T_N values found in these samples as compared to those of the NP samples.

ACKNOWLEDGMENTS

Fruitful discussions with Prof. L. Niinistö, Drs. H. Suematsu, T. Taniyama and Mr. M. Nagase are gratefully acknowledged. Mr. M. Matvejeff is acknowledged for his assistance in sample preparation and for performing some of the Mössbauer measurements. Mr. J. Nakamura is acknowledged for the synthesis of the Sm-based sample. One of the authors (J. L.) acknowledges kind support from the Japan Society for the Promotion of Science. The present work has been supported by a Grant-in-Aid for Scientific Research of contract No. 11305002 from The Ministry of Education, Science and Culture of Japan, and also by an International Collaborative Research Project Grant-1999 of the Materials and Structures Laboratory, Tokyo Institute of Technology.

REFERENCES

1. L. Er-Rakho, C. Michel, Ph. Lacorre, and B. Raveau, *J. Solid State Chem.* **73,** 531 (1988).
2. M. Pissas, C. Mitros, G. Kallias, V. Psycharis, A. Simopoulos, A. Kostikas, and D. Niarchos, *Physica C* **192,** 35 (1992).
3. V. Caignaert, I. Mirebeau, F. Bourée, N. Nguyen, A. Ducouret, J.-M. Greneche, and B. Raveau, *J. Solid State Chem.* **114,** 24 (1995).
4. M. Pissas, G. Kallias, V. Psycharis, H. Gamari-Seale, D. Niarchos, and A. Simoupoulos, *Phys. Rev. B* **55,** 397 (1997).
5. M. Nagase, J. Lindén, J. Miettinen, M. Karppinen, and H. Yamauchi, *Phys. Rev. B* **58,** 3371 (1998).
6. H. Yamauchi, M. Karppinen, and S. Tanaka, *Physica C* **263,** 146 (1996).
7. M. Karppinen and H. Yamauchi, *Mater. Sci. Eng.* **R26,** 51 (1999).
8. H. Yamauchi and M. Karppinen, *Physica C* **335,** 273 (2000).
9. M. Nagase, J. Lindén, H. Suematsu, M. Karppinen, and H. Yamauchi, *Phys. Rev. B* **59,** 1377 (1999).
10. P. Karen and P. M. Woodward, *J. Mater. Chem.* **9,** 789 (1999).
11. J. Lindén, P. Karen, A. Kjekshus, T. Pietari, and M. Karppinen, *Phys Rev. B* **60,** 15251 (1999).
12. J. Nakamura, J. Lindén, M. Karppinen, and H. Yamauchi, *Appl. Phys. Lett.* **77,** 1683 (2000).
13. K. Peitola, M. Kochi, M. Karppinen, H. Yamauchi, L. Niinistö, and J. Lindén, *J. Low Temp. Phys.* **119,** 861 (1999).
14. K. Lehmus, M. Kochi, M. Karppinen, H. Yamauchi, and L. Niinistö, *Int. J. Inorg. Mater* **2,** 203 (2000).
15. C. Meyer, F. Hartmann-Boutron, Y. Gros, and P. Strobel, *Solid State Commun.* **76,** 163 (1990).
16. H. Suematsu, M. Nagase, Y. Tomokiyo, M. Karppinen, and H. Yamauchi *in* "Advances in Superconductivity" Vol. XI, (N. Koshizuka and S. Tajima Eds.), pp. 389–392, Springer, Berlin, 1999.
17. R. J. Cava, A. W. Hewat, E. A. Hewat, B. Batlogg, M. Marezio, K. M. Rabe, J. J. Krajewski, W. F. Peck, Jr., and L. W. Rupp Jr., *Physica C* **165,** 419 (1990).
18. J. Lindén, A. Kjekshus, P. Karen, J. Miettinen, and M. Karppinen, *J. Solid State Chem.* **139,** 168 (1998).